

Electronically coupled complementary interfaces between perovskite band insulators

Mark Huijben¹, Guus Rijnders¹, Dave H.A. Blank¹, Sara Bals², Sandra Van Aert², Jo Verbeeck², Gustaaf Van Tendeloo², Alexander Brinkman¹, Hans Hilgenkamp¹

¹*Faculty of Science and Technology and MESA+ Institute for Nanotechnology, University of Twente, P.O. Box 217, 7500 AE Enschede, The Netherlands*

²*Electron Microscopy for Materials Research (EMAT), University of Antwerp, Groenenborgerlaan 171, 2020 Antwerp, Belgium*

Perovskite oxides exhibit a plethora of exceptional electronic properties, providing the basis for novel concepts of oxide-electronic devices^{1,2}. The interest in these materials is even extended by the remarkable characteristics of their interfaces. Studies on single epitaxial connections between the two wide-bandgap insulators LaAlO₃ and SrTiO₃ have revealed them to be either high-mobility electron conductors or insulating, depending on the atomic stacking sequences³. In the latter case they are conceivably positively charged. For device applications, as well as for basic understanding of the interface conduction mechanism, it is important to investigate the electronic coupling of closely-spaced complementary interfaces. Here we report the successful realization of such electronically coupled complementary interfaces in SrTiO₃ - LaAlO₃ thin film multilayer structures, in which the atomic stacking sequence at the interfaces was confirmed by quantitative transmission electron microscopy. We found a critical separation distance of 6 perovskite unit cell layers, corresponding to approximately 23 Å, below which a decrease of the interface conductivity and carrier density occurs. Interestingly, the high carrier mobilities characterizing the separate electron doped interfaces are found to be maintained in coupled structures down to sub-nanometer interface spacing.

Perovskite oxides are commonly described in terms of their cubic unit cells, with the generic formula ABO_3 . For a given parent compound, a rich phase diagram is colored-in by a substitution of the cations A or B, and/or a change in the oxygen stoichiometry. The ionic character of the chemical bonds and the consequent possibility of electronic reconstruction often render interfaces in these materials strongly electronically active. To understand this interface activity, it is instructive to describe the perovskites in terms of their constituting AO and BO_2 layering sequence. For example, whereas the two band-insulators $SrTiO_3$ and $LaAlO_3$ are seemingly similar, the SrO and TiO_2 layers are charge-neutral, while the charge states in the $LaAlO_3$ are $(LaO)^+$ and $(AlO_2)^-$, respectively. In heterostructures, the AO- BO_2 stacking sequence is maintained and consequently a polarity discontinuity arises at the $LaAlO_3$ - $SrTiO_3$ interface. It has been shown by Ohtomo and Hwang³ that due to this, the $LaO:TiO_2$ interface becomes conducting, and it is suggested that the conduction is governed by electron-transfer from $LaAlO_3$ into the TiO_2 bonds of the $SrTiO_3$. The complementary $AlO_2:SrO$ interface, with the AlO_2 possibly acting as an electron acceptor, remained insulating³. Such conducting interfaces are analogous to two-dimensional electron (hole) gases (2-DEGs) in semiconductors, which find applications in e.g., opto-electronic, high power RF and magnetoelectronic devices⁴. Great interest exists in the fundamental properties of electronically coupled 2-DEGs, placed very near to each other⁵.

Until now the investigations on the $LaAlO_3$ - $SrTiO_3$ interface conduction effects have concentrated on individual interfaces³. To study the electronic coupling of the complementary interfaces between these insulators, we fabricated high-quality multilayers in which a variable number of $LaAlO_3$ unit cell layers are stacked between $SrTiO_3$, and vice versa. The $LaAlO_3$ - $SrTiO_3$ heterostructures were grown by pulsed laser deposition, including in situ monitoring by Reflective High Energy Electron Diffraction (RHEED)⁶. Single-crystal $LaAlO_3$ and $SrTiO_3$ targets have been used, applying a KrF excimer laser at a repetition rate of 1 Hz and a laser fluency of ~ 1.3 J cm^{-2} . The deposition temperature was 850 °C, and the oxygen pressure 3×10^{-5} mbar.

The first type of heterostructure was deposited on TiO_2 -terminated $SrTiO_3$ (100) substrates⁷ and consisted of a $LaAlO_3$ layer followed by a $SrTiO_3$ top layer (Fig. 1a). Unit-cell RHEED intensity oscillations were used to control the number of unit cell

layers for both materials. The thickness of the LaAlO_3 layer was varied from 1 to 26 unit cells while the number of unit cells for the SrTiO_3 top layer was always kept constant at 10. As the internal polarization of the LaAlO_3 is the driver for the interface doping, a change of the LaAlO_3 layer thickness could possibly result in a modification of this polarization. For this reason we have also fabricated heterostructures of a second type, in which a thin SrTiO_3 layer is sandwiched between sufficiently thick LaAlO_3 layers (Fig. 1b). For the fabrication of those heterostructures, the TiO_2 -terminated SrTiO_3 (100) substrates were first covered with one monolayer of SrO by pulsed laser interval deposition⁸ at 50 Hz. Subsequently, a LaAlO_3 base-layer of 13 unit cells was deposited, followed by a SrTiO_3 layer, of which the thickness was varied from 2 to 11 unit cells, and finished by a LaAlO_3 top layer of 13 unit cells. Atomic force microscopy of the completed heterostructures showed atomically smooth terraces separated by unit cell steps, similar to the original substrate surface.

To examine the atomic stacking sequence at the interfaces, a superlattice of LaAlO_3 and SrTiO_3 was grown on a TiO_2 -terminated SrTiO_3 substrate. Figure 2a shows a high-angle annular dark field image (HAADF) taken along the [001] zone axis. In this image, which is obtained in a Titan 80-300 scanning transmission electron microscope (STEM), the intensities of the atomic columns scale with the atomic number Z . The weaker TiO and AlO columns are located in the center between respectively the brighter Sr and La columns. To investigate the atomic layers at the interface (e.g. $\text{AlO}_2\text{:SrO}$ or LaO:TiO_2) the signal-to-noise ratio is increased by averaging over the area indicated by the white rectangle in Figure 2a. This part of the image is divided into smaller subsections, which are added after cross correlation in Figure 2b. To quantitatively evaluate the peak heights of the atom columns, statistical parameter estimation is used, in which a parametric model of Gaussian peaks is fitted to Figure 2b in the least-squares sense. Figures 2c and 2d show the estimated peak heights corresponding to the La, Sr, TiO, AlO columns and the atom columns (X_A , X_B) at both interfaces (indicated in Fig. 2b). Also the 90% confidence intervals have been computed using the so-called Cramér-Rao lower bound⁹. Comparing the confidence intervals corresponding to the peak height of the atom columns at the interfaces with those of the surrounding TiO/AlO peaks confirms that the interface on top of every SrTiO_3 layer is $\text{TiO}_2\text{:LaO}$, whereas at the

bottom it is $\text{AlO}_2\text{:SrO}$. These configurations are also expected from the deposition parameters.

The electronic properties of the heterostructures were investigated by a four-point Van der Pauw method. For this, wire-bonded contacts were applied at the corners of the samples, connecting to the $(\text{AlO}_2)^-/(\text{SrO})^0$ interface as well as to the $(\text{LaO})^+/(\text{TiO}_2)^0$ interface. Measurements on individual interfaces using single LaAlO_3 layers on SrTiO_3 substrates confirmed the electron conduction of the $(\text{LaO})^+/(\text{TiO}_2)^0$ interface with a sheet conductance of $1.4 \times 10^{-4} (\Omega/\square)^{-1}$ at room temperature, while the $(\text{AlO}_2)^-/(\text{SrO})^0$ interface had a sheet conductance of $\sim 10^{-7} (\Omega/\square)^{-1}$. All single interface experiments showed photoconductivity due to photocarrier injection. Ultraviolet light illumination on single LaAlO_3 layers on SrTiO_3 substrates increased the conductivity by factors of 2 and 120 for the $(\text{LaO})^+/(\text{TiO}_2)^0$ and $(\text{AlO}_2)^-/(\text{SrO})^0$ interfaces, respectively. Conductance enhancements were only observed for wavelengths of the illuminated light below 380 nm, corresponding to the bandgap of 3.2 eV of SrTiO_3 . To enable a careful analysis of the intrinsic interface coupling, the effects of photocarrier injection were suppressed in the multilayer studies by shielding the samples from any light during the experiments and the 24 hours before.

The sheet resistances R_s at room temperature, for both types of heterostructures, are presented in Figure 3a for different values of the separation distance (d) between the two interfaces. A decrease in d is found to be accompanied by an increase in R_s below a separation distance of six unit cells, corresponding to 23 Å. Interestingly, both types of heterostructures show a similar dependence on the interface separation distance, albeit with a difference of 20% in the absolute value of R_s . The sheet carrier densities n_s were deduced from measurements of the Hall-coefficient R_H , using $n_s = -1/R_H e$. The room temperature results are shown in Figure 3b. Below a separation distance of six unit cells a decrease in sheet carrier density occurs for both types of heterostructures. The constant n_s for large d has a value of $\sim 1.8 \times 10^{14} \text{ cm}^{-2}$, corresponding to a charge density of $\sim 29 \mu\text{C cm}^{-2}$, which is ~ 0.27 electrons per unit cell area on the $(\text{LaO})^+/(\text{TiO}_2)^0$ interface. In this, the contribution by the $(\text{AlO}_2)^-/(\text{SrO})^0$ interface to the carrier density is neglected, due to its much lower conductivity.

The change in n_s and R_s below a certain interface separation distance relates to the charge distribution in the heterostructure. There exists no theoretical modelling yet of the SrTiO₃ – LaAlO₃ interface, to our knowledge, but it is interesting to make the comparison with interfaces between the Mott insulator LaTiO₃ and the band insulator SrTiO₃.¹⁰⁻¹² Notably, for that system a characteristic distance of 6 unit cells was predicted, over which charge transfer and electronic reconstruction takes place^{11,12}. The electronic reconstruction at a SrTiO₃-LaTiO₃ interface creates partially filled Ti-3d bands by band-bending effects and the symmetric confinement of charge leads to a suppression of n_s . An important difference with our experiments is the absence of TiO₂ layers in parts of our heterostructures. At the LaAlO₃ side, subbands are possibly created below the La-5d levels, in analogy with the Ti-3d levels at the SrTiO₃ side. The suppression of n_s , induced by the coupling between the interfaces, could then result from the constraint that the charge density at the (AlO₂)⁻/(SrO)⁰ interface is low.

The temperature dependence of the sheet resistance and the Hall coefficient provides further insight into the electronic properties of the interface electron gas. For the SrTiO₃/LaAlO₃/SrTiO₃ heterostructures the temperature dependence of the sheet resistance $R_s(T)$ is presented in Figure 4a for different values of the LaAlO₃ layer thickness (d_{LAO}) and Figure 4b shows the carrier density as determined from the Hall effect as function of temperature. The energy-scale over which charge carriers seem to be frozen out is 6.0 meV (Fig. 4c), which is comparable to observations in SrTiO₃ at low La-doping¹³. At temperatures above 100 K, the carrier density for $d_{\text{LAO}} = 2$ is approximately constant, for $d_{\text{LAO}} = 5$ the thermally activated increase continues.

The temperature dependence of the Hall mobility μ_H is given in Figure 4d. Above 50K the mobilities show a T^{-2} power law dependence, characteristic of Fermi-liquid behavior. Electron-phonon interactions are typically weak in SrTiO₃ (as is known from the poor heat conduction) and would give rise to a Bloch-Grüneisen temperature dependence of the resistance, which is not observed. Although electron-electron scattering is typically suppressed by screening and the Pauli exclusion principle, it is known to be relevant in transition metals with partially filled d-shells. At the n-type interface, this effect is expected to be important, when interface electronic reconstruction makes the Fermi surface intersect the Ti-3d subbands^{11,12,14}. For all

heterostructures, μ_H at room temperature is found to be constant at $6.0 \pm 1.0 \text{ cm}^2 \text{ V}^{-1} \text{ s}^{-1}$, without any dependence on the separation distances (d_{LAO} and d_{STO}). This value corresponds with room temperature mobilities reported for single interfaces^{3,15}. The very large mobilities in the zero-temperature limit provide an estimated electronic mean free path of $100 \text{ nm} - 1 \text{ }\mu\text{m}$. This large electronic mean free path and the fact that μ_H does not decrease for decreasing interlayer thickness indicates that electron scattering at impurities or crystalline defects in the nearby interface are not dominating effects for the mobilities at room temperature.

The studies on the $\text{LaAlO}_3\text{:SrTiO}_3$ heterostructures, presented above, prove the possibility to realize closely-spaced conducting sheets in these otherwise insulating oxide systems. This provides a perspective for novel all-oxide electronic devices as well as for basic studies. In this respect it is interesting to note that the employed growth techniques can also be applied to the fabrication of multilayers with exclusively n-type interfaces, by combining the SrTiO_3 and LaAlO_3 layers with single layers of LaTiO_3 or TiO_2 .

Acknowledgements

This work is part of the research program of the Foundation for Fundamental Research on Matter (FOM, financially supported by the Netherlands Organisation for Scientific Research (NWO)) and Philips Research. A.B., D.B., H.H. and G.R. acknowledge additional support from NWO. S.B. and S.V.A. are grateful to the Fund for Scientific Research-Flanders. The authors also acknowledge B. Freitag, A.J. Millis, Y. Ponomarev, F.J.G. Roesthuis, H. Rogalla, R. Wolters, W. van der Wiel, D. Veldhuis and FEI Company.

References

1. Ahn, C.H., Triscone, J.M. & Mannhart, J., *Nature* **424**, 1015 (2003).
2. Dagotto, E., *Science* **309**, 257 (2005).
3. Ohtomo, A. & Hwang, H. Y., *Nature* **427**, 423 (2004).
4. Ando, T., Fowler, A.B. & Stern, F., *Rev. Mod. Phys.* **54**, 437 (1982).
5. Eisenstein, J.P. & MacDonald, A.H., *Nature* **432**, 691 (2004)
6. Rijnders, G.J.H.M., Koster, G., Blank, D.H.A. & Rogalla, H., *Appl. Phys. Lett.* **70**, 1888 (1997).
7. Koster, G., Kropman, B.L., Rijnders, G.J.H.M., Blank, D.H.A. & Rogalla, H., *Appl. Phys. Lett.* **73**, 2920 (1998).
8. Koster, G., Rijnders, G.J.H.M., Blank, D.H.A. & Rogalla, H., *Appl. Phys. Lett.* **74**, 3729 (1999).
9. Den Dekker, A.J., Van Aert, S., Van den Bos, A. & Van Dyck, D., *Ultramicroscopy* **104**, 83 (2005).
10. Ohtomo, A., Muller, D.A., Grazul, J.L. & Hwang, H.Y., *Nature* **419**, 378 (2002).
11. Okamoto, S. & Millis, A. J., *Nature* **428**, 630 (2004).
12. Okamoto, S. & Millis, A. J., *Phys. Rev. B* **70**, 075101 (2004).
13. Okuda, T., Nakanishi, K., Miyasaka, S., Tokura, Y., *Phys. Rev. B* **63**, 113104 (2001).
14. Henrich, V.E., Dresselhaus, G. & Zeiger, H.J., *Phys. Rev. B* **17**, 4908 (1987).
15. Nishimura, J., Ohtomo, A., Ohkubo, A., Murakami, Y. & Kawasaki, M., *Jpn. J. Appl. Phys.* **43**, L1032 (2004).

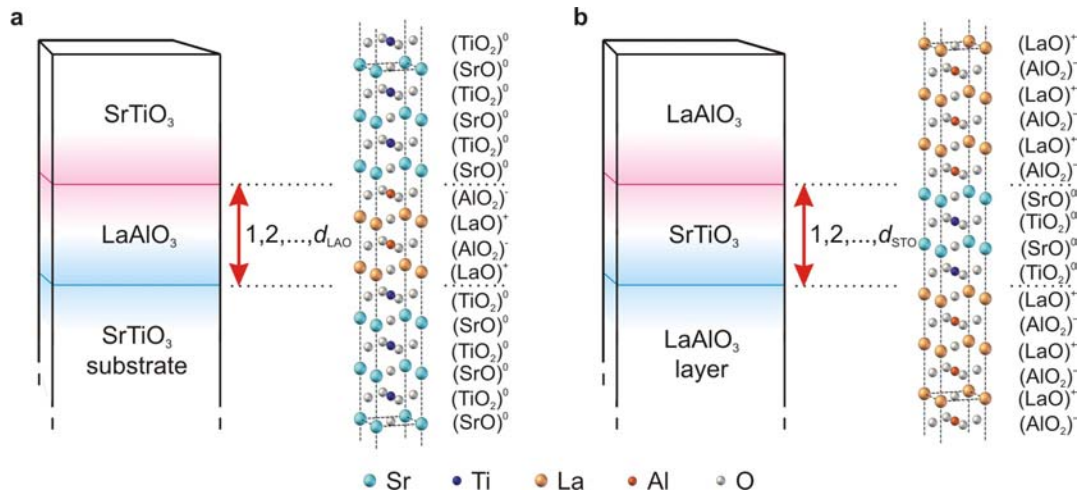


Figure 1. Representation of the investigated LaAlO₃/SrTiO₃ heterostructures. **a**, Schematic view of a SrTiO₃/LaAlO₃/SrTiO₃ heterostructure: a (001)-oriented LaAlO₃/SrTiO₃ bilayer grown on top of a TiO₂-terminated SrTiO₃ substrate, where the thickness of the LaAlO₃ layer (d_{LAO}) is varied. Atomic representation of the structure, showing the composition and charge state of each layer for the case of $d_{\text{LAO}} = 2$. **b**, Schematic view of a LaAlO₃/SrTiO₃/LaAlO₃ heterostructure: a (001)-oriented LaAlO₃/SrTiO₃/LaAlO₃ trilayer grown on top of a SrO-terminated SrTiO₃ substrate, where the thickness of the SrTiO₃ layer (d_{STO}) is varied. Atomic representation of the structure, showing the composition and charge state of each layer for the case of $d_{\text{STO}} = 2$.

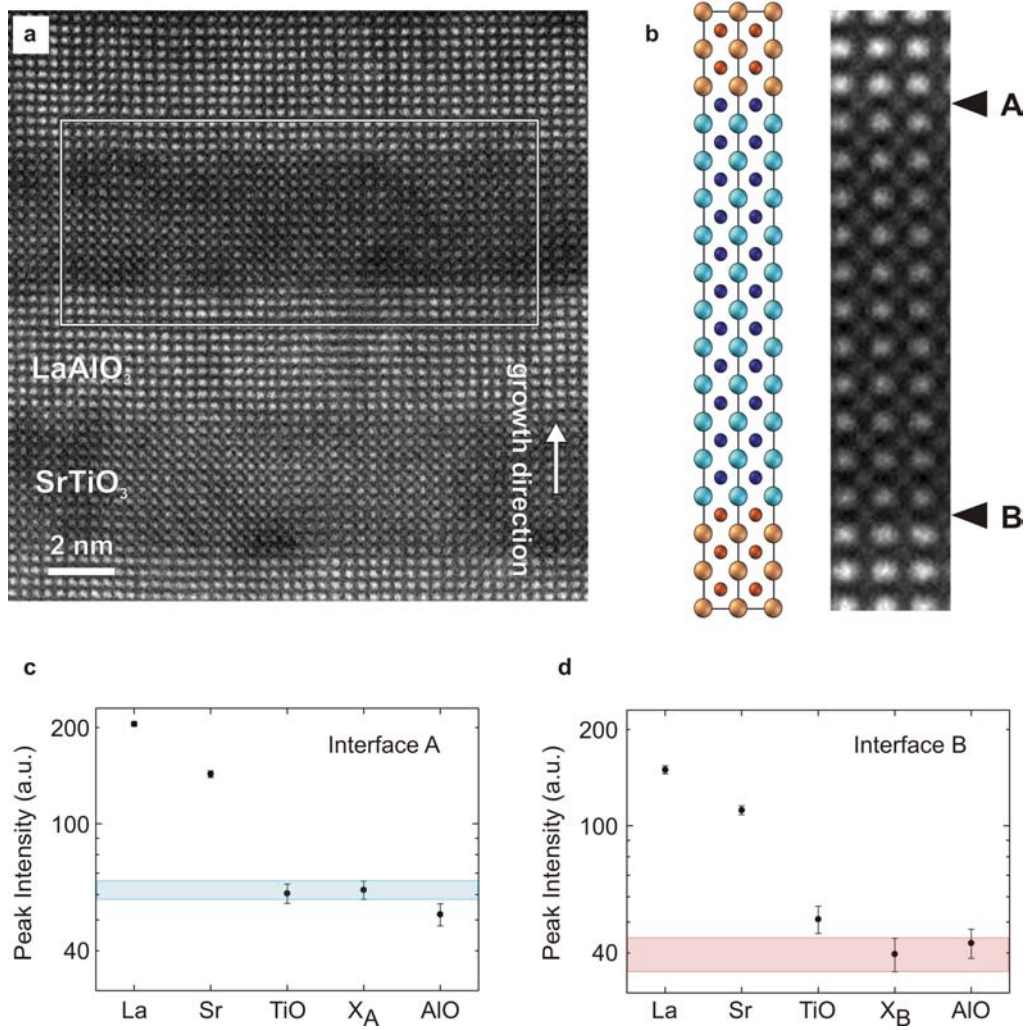


Figure 2. Quantitative scanning transmission electron microscopy analysis of the atomic stacking sequences at the interfaces. **a**, High-angle annular dark field (HAADF) image of the LaAlO₃/SrTiO₃ superlattice along the [001] zone axis. The area of the image indicated by the white rectangle is used for averaging. **b**, Image showing the result of the averaging procedure, together with the atomic representation of the structure. The atomic positions are indicated in size and color as in Fig. 1. The image is used as a starting point for quantitative peak estimation of the La, Sr, TiO, AIO columns and of the atom columns at the interfaces (indicated with A and B). **c+d**, The estimated peak heights of the La, Sr, TiO, AIO columns and of the atom columns at the interfaces (indicated with symbols X_A and X_B) together with the corresponding 90% confidence intervals. The colored bands indicate the 90% confidence intervals of the atom columns at the interfaces (X_A and X_B).

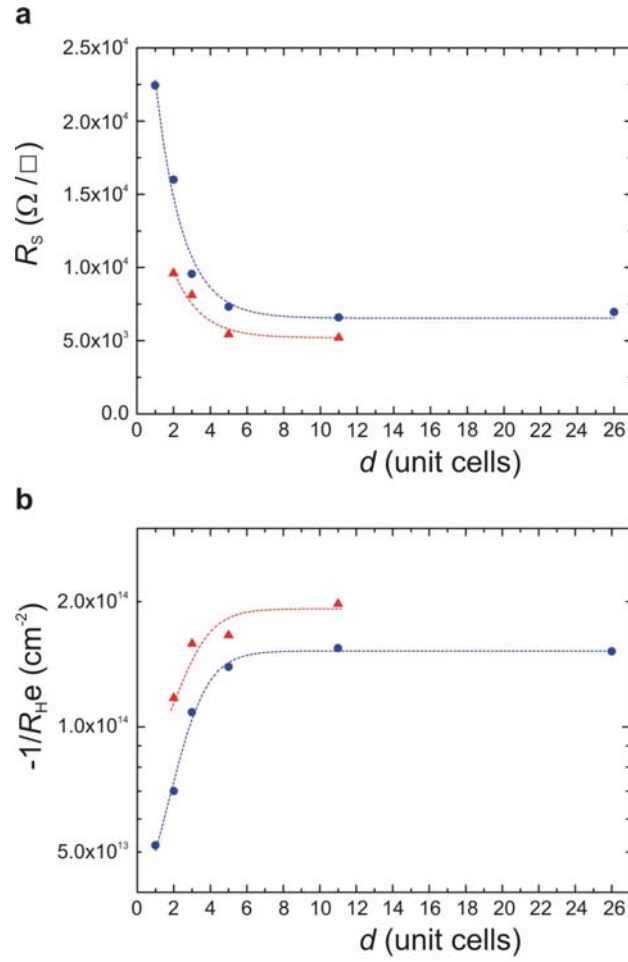


Figure 3. Electronic properties of the $\text{LaAlO}_3/\text{SrTiO}_3$ heterostructures at 300 K for different separation distances between the interfaces. **a**, Dependence of the sheet resistance R_s on the separation distance d . **b**, Dependence of $-1/R_H e$ on the separation distance d . $\text{SrTiO}_3/\text{LaAlO}_3/\text{SrTiO}_3$ heterostructures and $\text{LaAlO}_3/\text{SrTiO}_3/\text{LaAlO}_3$ heterostructures are indicated by circles and triangles, respectively. The dashed lines are guides to the eye.

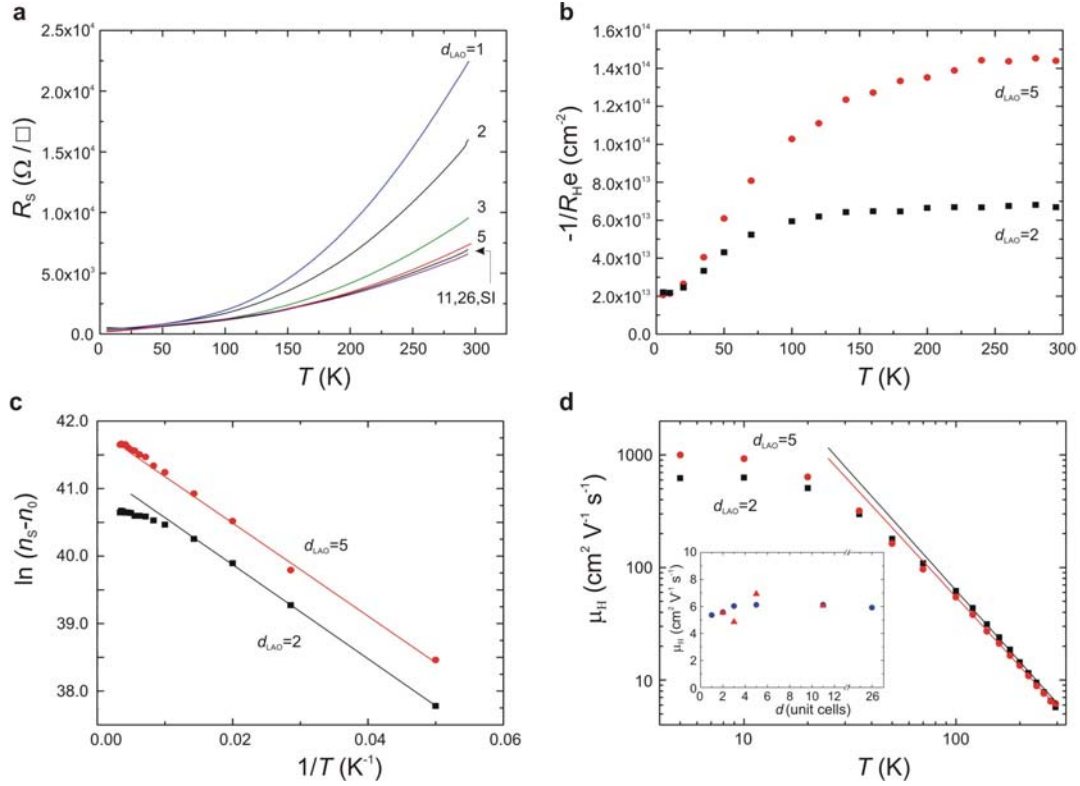


Figure 4. Transport properties of the LaAlO₃/SrTiO₃ heterostructures for different separation distances between the interfaces. **a**, The temperature dependence of the sheet resistance $R_s(T)$ for different thicknesses of the LaAlO₃ layer (d_{LAO}) in SrTiO₃/LaAlO₃/SrTiO₃ heterostructures. A measurement on a single (LaO)⁺/(TiO₂)⁰ interface (SI) is also indicated. **b**, Temperature dependence of $-1/R_H e(T)$ for SrTiO₃/LaAlO₃/SrTiO₃ heterostructures with separation distances of $d_{\text{LAO}} = 2$ (squares) and 5 (circles). **c**, Temperature dependence of $\ln(n_s - n_0)$ for SrTiO₃/LaAlO₃/SrTiO₃ heterostructures with separation distances of $d_{\text{LAO}} = 2$ (squares) and 5 (circles), where n_s is defined as $-1/R_H e$ and n_0 is the low temperature limit of n_s . **d**, Temperature dependence of Hall mobility $\mu_H(T)$ for SrTiO₃/LaAlO₃/SrTiO₃ heterostructures with separation distances of $d_{\text{LAO}} = 2$ (squares) and 5 (circles). The inset shows the separation distance d dependence of $\mu_H(T)$ at 300 K, where SrTiO₃/LaAlO₃/SrTiO₃ heterostructures and LaAlO₃/SrTiO₃/LaAlO₃ heterostructures are indicated by circles and triangles, respectively.